Volume 1 | Number 1 | Jan 2013 | Pages 1–100

# Polymer Chemistry

www.rsc.org/polymers

ROYAL SOCIETY OF CHEMISTRY

ROYAL SOCIETY OF CHEMISTRY

www.rsc.org/polymers

# Polymer Chemistry

## ARTICLE

# Functional, sub-100 nm polymer nanoparticles *via* thiol-ene miniemulsion photopolymerization

D.V. Amato,[a] D. N. Amato,[a] A. S. Flynt,[b] and D. L. Patton*[a]

In this work, sub-100 nm crosslinked polythioether nanoparticles were synthesized *via* thiol-ene photopolymerization in miniemulsion using high-energy homogenization. The effects of the miniemulsion formulation and homogenization parameters – including inhibitor concentration, surfactant concentration, organic weight fraction, ultrasonication time and amplitude – on nanoparticle size and size distribution were investigated. Thiol-ene nanoparticles with a mean particle diameter of 46 nm were obtained under optimized conditions for the current system at 2.5 wt. % organic fraction and 20 mM surfactant concentration. In an effort to demonstrate potential utility of thiol-ene nanoparticles, we exploit the step-growth radical mechanism of thiol-ene photopolymerization under non-stoichiometric conditions to fabricate functional nanoparticles that express excess thiol or alkene at the particle surface. We show that these excess functional groups can be utilized as reactive handles in thiol-Michael and radical-mediated thiol-ene reactions for immobilization of fluorescent moieties *via* postpolymerization modification.

## 1. Introduction

Polymer nanoparticles with tunable functionality have emerged as a promising and viable technology platform for applications including coatings, cosmetics, nanomedicine, and imaging. The prospects of advancing these and other technologies have provided great impetus for the development of rapid, low-cost methodologies for the synthesis of functional polymer nanoparticles – particularly with sizes less than 100 nm. Polymer nanoparticles have been prepared by two general routes: 1) postpolymerization processing, including nanoprecipitation, dialysis, and supercritical fluid expansion, and 2) direct polymerization of monomers or crosslinking of macromers in dispersed heterophase systems, including microfluidics, microemulsion, and miniemulsions.[1] Miniemulsions – with droplet sizes typically in the range of 20-200 nm – are particularly well-suited for the synthesis of small polymer nanoparticles.[2, 3] Miniemulsions are non-equilibrium systems created under high shear conditions (i.e. ultrasonication or high-pressure homogenization) yielding small, narrowly distributed droplets stabilized by a surfactant and costabilizer (or hydrophobe) in a continuous phase.[4] Unlike conventional emulsion polymerization, initiation and particle nucleation occur predominately in droplets, which serve as discrete nanoreactors, enabling the preservation of size and composition of each droplet during polymer synthesis.[2]

While miniemulsion polymerizations have predominately been conducted using radical chain growth mechanisms, several examples have highlighted the utility of various step-growth mechanisms – particularly step-growth polyaddition polymerizations.[5, 6] The earliest work focused on classic polyaddition reactions in miniemulsion, such as diamine/epoxide[7] and diisocyanates/diols.[8] More recently, the focus has shifted to "click" polyaddition reactions in miniemulsions for the synthesis of polymer microparticles, nanoparticles, and nanocapsules. Landfester *et al.*[9] employed miniemulsion copper-mediated and copper-free azide-alkyne 1,3-dipolar cycloaddition (CuAAC) interfacial polymerization for the synthesis of polytriazole nanocapsules. Similarly, Bernard *et al.*[10] reported interfacial CuAAC miniemulsion polymerization of diazides and dialkynes under microwave irradiation to achieve glyconanocapsules with high conversion (>98%) in under 30 min.

In addition to CuAAC, thiol-mediated chemistries (i.e. thiol-ene/yne, thiol-Michael) represent an attractive family of "click" polyaddition reactions for rapid fabrication of microparticles and nanoparticles in dispersed heterophase systems, as these reactions generally proceed under mild conditions with high efficiency and rapid reaction kinetics.[11-13] For radical-mediated thiol-ene reactions, the thioether product forms *via* a free-radical step-growth process facilitated by a rapid, highly efficient chain transfer reaction between multifunctional alkenes and thiols, which provides insensitivity to oxygen and water. The earliest examples of thiol-ene related miniemulsions involved surface functionalization of residual alkenes with PEG-thiol on styrene/divinylbenzene composite nanoparticles,[14] and

crosslinked biodegradable nanoparticles composed of allyl-functionalized polylactide with a difunctional thiol.[15] Regarding direct polymerization of thiol-ene in disperse heterophase systems, Shipp and coworkers[16] recently reported the first example of crosslinked polythioether microparticles synthesized via thiol-ene suspension photopolymerization. Shipp's initial work focused on the effects of surfactant concentration, cosolvent, and mixing on microparticle formation, while subsequent work explored the dependence of microparticle size and stability on surfactant structure.[17] These initial examples clearly illustrated the utility of thiol-ene photopolymerization for creating microparticles with rapid reaction rates, high monomer conversion and homogeneous network structure in dispersed systems; however, Shipp's work focused minimally on the use of high-energy ultrasonication for the preparation of small thiol-ene nanoparticles. Similarly, Zhang et al.[18] reported thiol-ene suspension photopolymerization for the synthesis of large (> 200 μm) porous microparticles using PMMA as a porogen. In 2014, Jasinski et al.[19] reported thiol-ene photopolymerization in miniemulsion using a difunctional thiol and a difunctional alkene yielding linear poly(thioether ester) nanolatex particles with 130 nm diameter and 55% crystallinity. The authors demonstrated the formation of clear, chemically resistant, and elastomeric films upon evaporation of water from the cured dispersions. It is also noteworthy to mention recent work by Bowman et al.[20] that utilized thiol-Michael polyaddition reactions in dispersion polymerization to fabricate monodisperse microspheres (>1 μm) from multifunctional thiols and Michael acceptors. Bowman importantly showed the ease by which fluorescent microspheres could be prepared via postpolymerization modification using off-stoichiometric conditions. Considering the relatively few examples of thiol-mediated polyadditions in dispersed systems, and the primary focus of these works on either microparticles or linear nanolatex particles, a significant opportunity remains to exploit thiol-mediated polyadditions in miniemulsion for the fabrication of crosslinked, functional polymer nanoparticles.

Herein, we report the synthesis of small, sub-100 nm polythioether nanoparticles using miniemulsion thiol-ene photopolymerization. We specifically focus on tailoring the miniemulsion formulation (inhibitor, surfactant concentration, monomer weight fraction) and processing parameters (ultrasonication time and amplitude) to achieve nanoparticles with diameters in the sub-100 nm range with relatively narrow size distributions. In contrast to previous work by Shipp[16] and Jasinski,[19] we found the inclusion of a radical inhibitor in the thiol-ene formulation to be critically important in preventing premature polymerization during ultrasonic emulsification – prior to exposure to UV light. In an effort to demonstrate potential utility of thiol-ene nanoparticles, we exploit the step-growth radical mechanism of thiol-ene photopolymerization under non-stoichiometric conditions to fabricate functional nanoparticles that express excess thiol or alkene at the particle surface. We show that these excess functional groups can be utilized as reactive handles in thiol-Michael and radical-
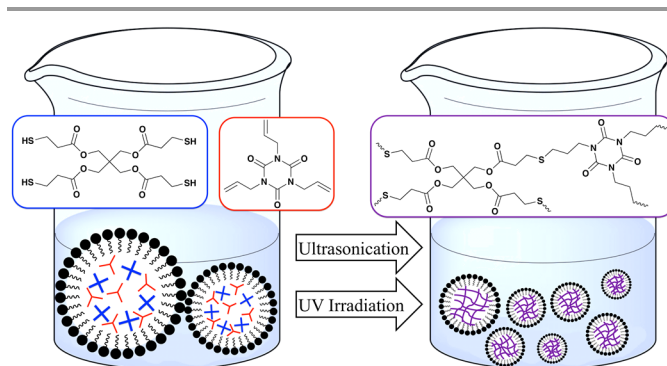


Figure 1. Thiol-ene precursors and miniemulsion process for preparing sub-100 nm polythioether nanoparticle via photopolymerization.

mediated thiol-ene reactions for immobilization of fluorescent moieties via postpolymerization modification.

## 2. Experimental

### 2.1 Materials

Hexadecane, 1,3,5-triallyl-1,3,5-triazine-2,4,6 (1H, 3H, 5H) trione (TTT), 4-p-methoxy phenol (MEHQ), sodium dodecyl sulfate (SDS), 2,2-dimethoxy-2-phenylacetophenone (DMPA), tetrahydrofuran (THF), 7-mercapto-4-methylcoumarin and butyl acetate (Sigma-Aldrich), pentaerythritol tetra(3-mercaptopropionate) (PETMP, BrunoBock), 1-hydroxycyclohexyl phenyl ketone (Irgacure 184, CIBA), and Texas Red® C2 maleimide (Invitrogen) were obtained at the highest purity available and used without further purification unless otherwise specified.

### 2.2 General Sample Preparation

Each sample was prepared in a 20 mL scintillation vial with a total volume 10 mL. The organic stock solution shown in Table 1 was added into the vial containing a stock solution of SDS and deionized water. The samples were then placed into an ice bath.

**Table 1.** General formulation of organic stock solution for thiol-ene photopolymerization in miniemulsion.

| Organic Fraction | Mass (g) | Wt. % |
|---|---|---|
| Hexadecane | 0.439 (1.94 mmol) | 4.72 |
| TTT | 1.52 (6.10 mmol) | 16.3 |
| PETMP | 2.22 (4.53 mmol) | 23.8 |
| Irgacure 184® | 0.100 (0.49 mmol) | 1.07 |
| 4-p-methoxy phenol | 0.030 (0.24 mmol) | 0.322 |
| Butyl acetate | 5.00 (43.04 mmol) | 53.7 |

and sonicated using a Q-700A-110 probe ultrasonicator at 5-25% amplitude for 5-45 minutes. The miniemulsions were then cured using an Omnicure S1000-1B with a 100W mercury lamp (λ$_{max}$=365 nm, 320-500 nm filter) and an intensity of 185 mW/cm$^2$ for 10 minutes unless noted otherwise. All samples were made in triplicate to ensure reproducible data. To optimize the formulation for small nanoparticles, the organic fraction was

varied with a constant SDS concentration of 20 mM. The SDS stock formulation and tabulated samples prepared are listed in Table SI-1 and SI-2.

### 2.3 Preparation of nanoparticles with excess thiol and excess alkene

Nanoparticles with excess thiol were prepared using a 1.5:1 thiol to alkene stoichiometry, for example, PETMP (2.8 g, 5.73 mmol) and TTT (0.95 g, 3.81 mmol). The remaining constituents in the organic formulation from Table 1 were held constant. To the scintillation vial, 250 µL of organic solution was pipetted into 9.75 mL of 20 mM SDS in DI water. The sample was then ultrasonicated for 20 minutes at 10% amplitude and cured under UV light for 10 minutes. Nanoparticles containing excess alkene were similarly synthesized using a 2:1 alkene to thiol ratio, i.e. TTT (2.15 g, 8.63 mmol) and PETMP (1.58 g, 3.23 mmol).

### 2.4 Fluorescent tagging of excess thiol nanoparticles

From the nanoparticle suspension (10 mL) with excess thiol prepared in 2.3, 2 mL were removed and placed into a 20 mL scintillation vial wrapped in aluminum foil with a stir bar. A stock solution of Texas Red® C2 maleimide was made by addition 10 µL of Texas Red® C2 maleimide to 100 µL of DMSO. 50 µL of the Texas Red® C2 maleimide stock solution was added to the nanoparticles and stirred overnight. The nanoparticle were purified by centrifugation (5 minutes at 13,300 rpm, Fisher Scientific™ accuSpin™ Micro 17 centrifuge) to remove unreacted Texas Red® C2 maleimide. The supernatant was removed and the nanoparticle pellet was re-suspended in 1 mL DI water. The nanoparticle suspension was then cast onto a glass slide and allowed to dry at room temperature. The resulting slide was analyzed using a Zeiss LSM 510 confocal laser scanning microscope ($\lambda_{ex}$=543 nm).

### 2.5 Fluorescent tagging of excess alkene nanoparticles

From the nanoparticle suspension (10 mL) with excess ene prepared in 2.3, 1 mL was removed and centrifuged for 18 min at 13,300 rpm. The supernatant was removed and the nanoparticle pellet was re-suspended in 1 mL of THF. A solution was prepared containing 80 mg of 7-Mercapto-4-methylcoumarin, 30 mg of DMPA and 1 mL of THF was added. The solutions were combined and exposed to UV light for 5 minutes to induce the radical thiol-ene reaction. The solution was centrifuged for 10 minutes, supernatant removed, the pellet re-suspended in THF. The coumarin-functionalized nanoparticles were then cast onto a glass slide with a coverslip for analysis by confocal laser scanning microscopy ($\lambda_{ex}$=405 nm).
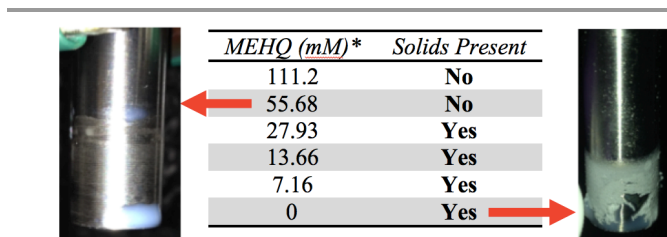
### 2.6 Characterization

The size and distribution of the nanoparticles were measured by dynamic light scattering (DLS) using a Microtrac Nanotrac Ultra NPA150. Particle size and distribution were obtained using the Microtrac Flex software (v.10.6.1), which employs non-negatively constrained least-squares (NNLS) and cumulants analysis to obtain the intensity-weighted "z-average" mean particle size as the first cumulant, and the polydispersity index

from the second cumulant.[21] Transmission electron micrographs (Digital Imaging with Gatan Model 785 ES1000W Erlangshen CCD Camera) were taken with a Zeiss 900 TEM operating at 50kV. Samples were applied to 200 mesh copper grids (3.05 mm, 200 lines/inch square mesh, EMS Cat. #G200-Cu) coated with Formvar (5% polyvinyl formal resin). The samples were then stained using $OsO_4$. Atomic force microscopy (AFM) was performed using a Bruker Icon in tapping mode. The samples were imaged with T300R-25 probes (Bruker AFM Probes) with a spring constant of 40 Nm[-1]. ^{1}H NMR was recorded on a Varian Mercury Plus 300 MHz NMR in $D_2O$. FTIR was conducted using a Nicolet 8700 spectrometer with a KBr beam splitter and a liquid nitrogen cooled MCT/A detector.

## 3. Results and Discussion

Thiol-ene polymer nanoparticles were synthesized *via* ultrasonication of a dispersed organic phase into an aqueous solution of surfactant, as shown in Figure 1. The horn was inserted into a glass vial and the organic phase was emulsified into the aqueous phase while a secondary ice bath was placed around the vial to prevent overheating. Samples prepared without ice resulted in larger particles and coagulum formation on the horn tip.

Thiol-ene miniemulsions were prepared by adding an organic phase containing monomers (TTT and PETMP), photoinitiator, hydrophobe, inhibitor, and solvent to an aqueous phase consisting of water and surfactant (SDS). Butyl acetate was chosen as the solvent because it is close to being isorefractive with water which could lower the final turbidity of the miniemulsion.[22] Hexadecane was chosen, as it is known to help prevent Ostwald ripening and increase the lifetime of the miniemulsion. The organic phase once mixed was then emulsified in the aqueous phase *via* ultrasonication to create nanodroplets.



| MEHQ (mM)* | Solids Present |
|---|---|
| 111.2 | No |
| 55.68 | No |
| 27.93 | Yes |
| 13.66 | Yes |
| 7.16 | Yes |
| 0 | Yes |

*concentration relative to 5 grams of butyl acetate.

**Figure 2.** Influence of inhibitor concentration (MEHQ) on preventing polymerization during ultrasonic homogenization.

Our initial attempts to synthesize sub-100 nm thiol-ene nanoparticles using probe ultrasonication under conditions described in the literature (i.e. in the absence of radical inhibitor as reported by Shipp *et al*.[16]) resulted in the formation of solids in solution and on the surface of the horn during ultrasonication, prior to exposure to UV light, presumably due to thermally-induced polymerization. As a result of these observations, we introduced a radical inhibitor – MEHQ – into the organic phase and investigated the effect of inhibitor concentration on the
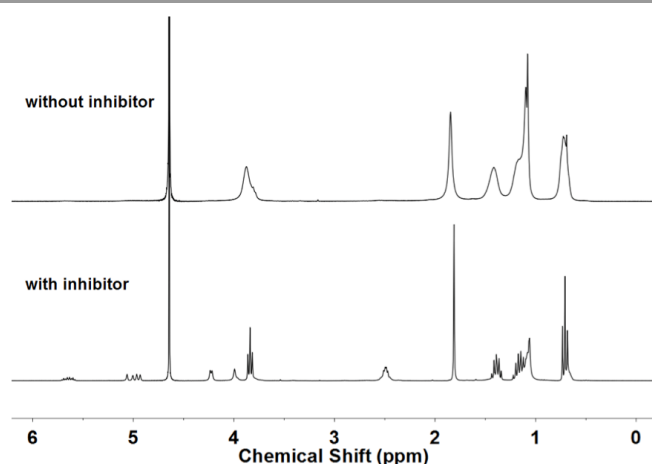
**Figure 3.** Typical $^1$H NMR spectra of ultrasonicated samples with and without inhibitor.

miniemulsion process. MEHQ was chosen because it is a commonly used stabilizer for alkene containing monomers. The MEHQ concentration in the organic phase was varied according to values shown in Figure 2, where the minimum concentration that inhibited latex formation was found to be 55.7 mM. MEHQ concentrations below this minimum threshold resulted in the formation of solids on the surface of the ultrasonic horn, as shown in Figure 2. To further probe the ability of the inhibitor to prevent premature polymerization during the emulsification process, thiol-ene miniemulsions with and without inhibitor were prepared using a deuterium oxide/SDS solution as the continuous phase. Upon ultrasonication, an aliquot of sample was removed and analyzed *via* $^1$H NMR, while the remaining fraction of the sample was photopolymerized under UV light prior to collecting a second aliquot for analysis. Figure 3 shows the NMR spectra of thiol-ene miniemulsions with and without MEHQ prior to UV exposure. The sample with MEHQ showed the typical proton resonances for the unreacted alkene of TTT at 4.92–5.15 ppm and 5.58–5.75 ppm, and a resonance for an unreacted mercaptopropionate ($-CH_2CH_2-SH$) at 2.51 ppm. Devoid of MEHQ, the miniemulsion shows complete disappearance of the alkene and thiol monomer peaks, and exhibits peak broadening indicative of polymerization. These results provide evidence that the uninhibited sample undergoes polymerization through the sonochemical cavitation process, and that MEHQ is required to prevent premature polymerization. These observations are supported by the work of Skinner *et al.*,[23] which quantified room temperature sonochemical initiation in thiol-ene systems using a radical trap (2,2-diphenyl-1-picryhydrazyl), and showed a radical generation at a rate of $0.62 \times 10^{-4}$ mol dm$^{-3}$ s$^{-1}$ led to successful thiol-ene reactions even in the absence of a radical initiator. Therefore, MEHQ plays a critical role in the current thiol-ene miniemulsion system to prevent simultaneous occurrence of monomer droplet formation and polymerization – a process that could lead to broad particle size distributions and uncontrolled process parameters. It is also important to note that the inhibitor has a minimal effect on the thiol-ene photopolymerization process. Exposure of the inhibited thiol-ene
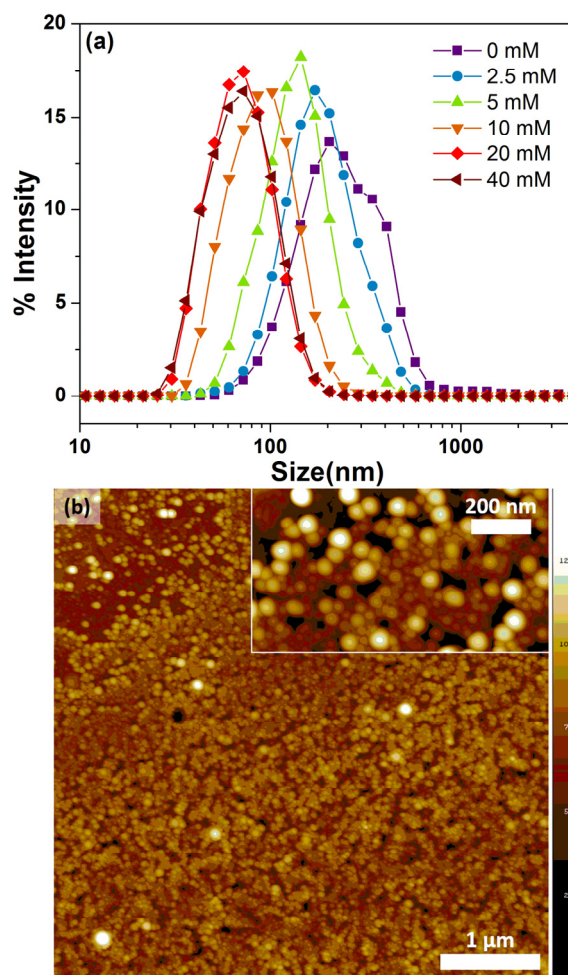


**Figure 4.** (a) Effect of SDS concentration on nanoparticle size distribution. (b) Representative tapping mode AFM image of thiol-ene nanoparticles obtained at 20 mM SDS by evaporation of a droplet of the photocured miniemulsion (Synthetic conditions: 2.5 wt.% organic, 20 min ultrasonication at 10% amplitude, 10 min UV exposure).

miniemulsions to UV light results in high monomer conversion (>99%), as indicated by complete disappearance of the peaks associated with the thiol (2567 cm$^{-1}$) and alkene (3082 cm$^{-1}$) functional groups in FTIR of the cured samples (see Figure S1).

The stability and size of monomer droplets, and ultimately polymer nanoparticles, obtained from heterogeneous miniemulsion polymerizations are strongly influenced by several process parameters, including surfactant structure and concentration, organic phase volume fraction, and the presence of a costabilizer. To explore the effect of SDS concentration on nanoparticle size, the concentration of SDS was varied from 0 to 40 mM, while keeping the organic fraction and composition constant. As shown in Figure 4a, thiol-ene miniemulsions carried out in the absence of SDS provided a mean particle size of 145 nm and a broad, multimodal particle size distribution (PDI: 0.338). With increasing SDS concentration, the mean particle size systematically decreased due to an increase in surfactant interfacial area and a decrease in interfacial tension enabling stabilization of smaller nanodroplets. 20 – 40 mM SDS
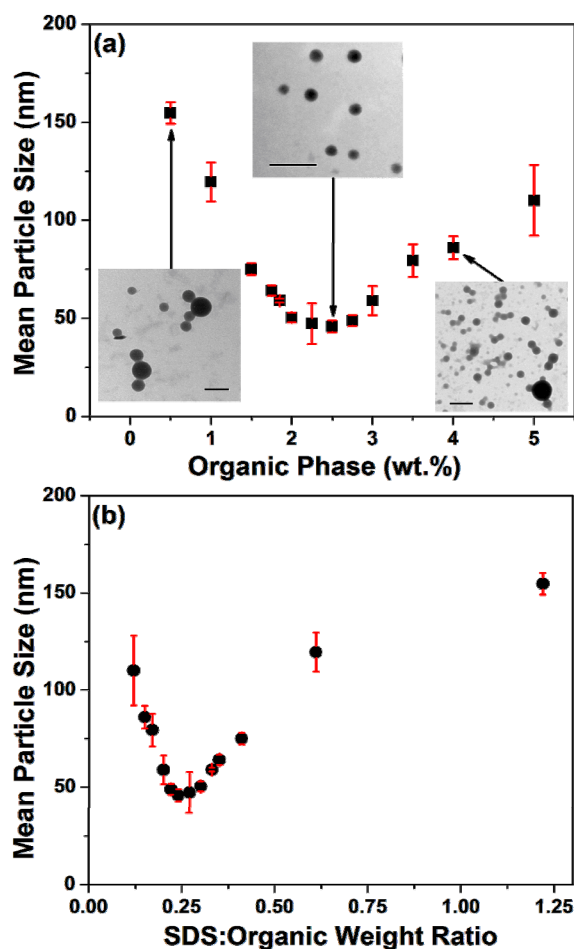
**Figure 5.** Dependence of the nanoparticle size on (a) organic weight fraction and (b) SDS:organic ratio. The (a) insets show representative TEM images of UV cured miniemulsions at various organic weight fractions (scale bar length = 200 nm). (Synthetic conditions: 20 min ultrasonication at 10% amplitude, 10 min UV exposure).



**Figure 6.** Effect of SDS:organic ratio on mean nanoparticle size. (Synthetic conditions: 20 min ultrasonication at 10% amplitude, 10 min UV exposure).

provided thiol-ene nanoparticles with a mean particle size of 55 nm and relatively narrow particle size distributions (PDI: 0.255). A significant difference in particle size between 20 mM and 40 mM SDS was not observed, thus 20 mM SDS was used in all other formulations. Figure 4b shows a representative tapping mode AFM image of thiol-ene nanoparticles obtained by evaporation of a droplet of the photocured miniemulsion (20 mM SDS). As expected, the nanoparticles are spherical in shape and exhibit a ranges of particle sizes that agree with the DLS results.

The effect of organic weight fraction on the particle size was examined next. For these experiments, the concentration of SDS was kept constant (20 mM), while the organic weight fraction was varied from 0.5 – 5 wt. % relative to the aqueous phase. These conditions also correlate to a varying *SDS:organic* weight ratio from 0.12 – 1.22. The results from these experiments are shown in Figures 5a and 5b, which relate mean particle size to the organic weight fraction and *SDS:organic* ratio, respectively. Percent transmission and photographs of the minemulsions described above are shown in Figure S3. The smallest mean particle size (46 nm) was obtained from a system containing 2.5
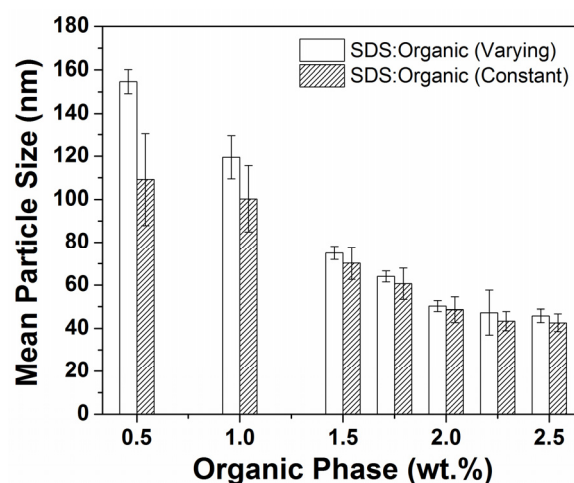
wt. % organic phase. The corresponding TEM image for the 2.5 wt. % sample shows well-defined thiol-ene nanoparticles with sizes that are in good agreement with values obtained by DLS (see Figure S2 for lower magnification TEM image). Increasing the organic weight fraction from 2.5 wt. % resulted in an increase in the mean particle size, as shown in Figure 5a. A larger particle size with increasing organic fraction is likely due to depletion of free SDS required to stabilize the smaller nanodroplets.[24] With overall SDS concentration held constant at 20 mM, the SDS:organic ratio, as shown in Figure 5b, decreases with increasing organic fraction enabling droplet coalescence and ultimately larger nanoparticles. Likewise, decreasing the organic weight fraction from 2.5 wt. % resulted in an increase in nanoparticle size (up to 155 nm at 0.5 wt. %). In this case, the *SDS:organic* ratio increases from 0.24 at 2.5 wt. % organic to 1.22 at 0.5 wt. % organic representing an excess of SDS, as shown in Figure 5b. Consequently, destabilization and coalescence of small droplets may be caused by attractive forces between multiple nanodroplets in the presence of excess surfactant – a phenomenon that follows a similar mechanism as described in depletion flocculation.[25, 26]

Additionally, excess surfactant can facilitate Ostwald ripening via the diffusion of organic soluble constituents from smaller droplets, across the aqueous phase, into larger droplets. Interestingly, thiol-ene miniemulsions prepared at various organic weight fractions (0.5 – 2.5 wt. %) with constant surfactant to organic ratios also exhibited a decrease in nanoparticle size with increasing organic weight fraction, as shown in Figure 6. Such behavior is indicative of a $\tau_1$ mechanism, or an osmotically controlled steady-state droplet size driven by Ostwald ripening – as opposed to a steady-state controlled by collision rates and colloidal stability ($\tau_2$ mechanism).[27] The apparent $\tau_1$ mechanism observed here may be attributable to the choice of butyl acetate as a solvent for the thiol-ene monomer phase. The relatively high solubility of butyl acetate in water may promote exchange of monomers through

the aqueous phase *via* Ostwald ripening.  This interesting behavior will require additional investigation; however, we note that interest in such low (i.e. < 2.5 wt. %) solids content is likely minimal – particularly from nanoparticle yield viewpoint.

Figure 7 illustrates the importance of the costabilizer – hexadecane – on droplet stabilization directly following the formation of the miniemulsion *via* ultrasonication, particularly when employing butyl acetate as a solvent for the monomer phase.  Thiol-ene miniemulsions prepared with and without hexadecane as a costabilizer were allowed to equilibrate for various times prior to photopolymerization.  As shown in Figure 7, samples prepared with hexadecane exhibited a relatively stable mean particle size over a 72 h period, and provided thiol-ene miniemulsions with translucent optical properties (Figure 7, inset).  In the absence of hexadecane, the miniemulsions were highly unstable and resulted in the formation of precipitants that settled to the bottom of the vial upon cure.  For this reason, DLS
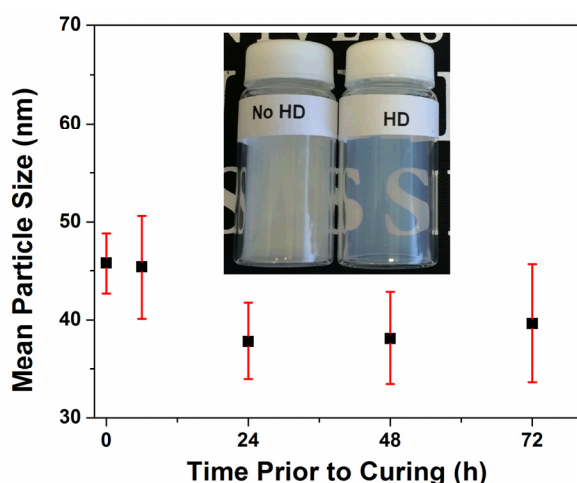


**Figure 7.** Effect on the presence of hexadecane for samples that were ultrasonicated and then cured after three hours (Synthetic conditions:  20 mM SDS, 2.5 wt.% organic, 20 min ultrasonication at 10% amplitude, 10 min UV exposure).

measurements for samples without hexadecane were not representative of the full particle distribution and were not included in Figure 7.  The "no HD" vial in the Figure 7 inset image clearly shows an opaque suspension of thiol-ene particles. Hexadecane functions to prevent Ostwald ripening by retarding monomer and solvent diffusion from small droplets to large droplets.

In addition to the effect of formulation parameters (i.e. surfactant concentration, organic fraction, etc.) on nanoparticle size, we also elucidated the evolution of particle size as a function of processing parameters, such as ultrasonication time and amplitude.  Ultrasonication experiments were carried out on samples with a constant formulation, namely samples containing 2.5 wt. % organic phase and a constant *SDS:organic* ratio of 0.25.  Figure 8a shows the evolution of nanoparticle size with ultrasonication time at 10% amplitude for processing times ranging from 5 – 45 minutes.  As sonication time was increased, the particle size decreased from 82 nm at 5 min to 36 nm at 45

min.   Homogenization times beyond 45 min, at constant composition and amplitude, resulted in no further decreases in particle size.  It is important to note here that an ice bath was employed to keep the samples cool during the ultrasonication process.  For example, the bulk temperature of the reaction media typically showed a 10 °C increase after 20 min of ultrasonication at 10% amplitude.  Allowing the miniemulsions to further increase in temperature with extended sonication times resulted in reduced control over particle size and poor repeatability. Figure 8b shows the progression of mean particle size after 20 min of ultrasonication at various sonication powers (% amplitude).   Similarly to increasing the duration of ultrasonication, it was found that a particle size of 35 nm could be obtained at 20% amplitude in half the time observed for experiments conducted at 10% amplitude.  Similar trends were reported by Delamas *et al.*[28] for ultrasonic processing of small miniemulsions, where the equilibrated particle size was found to be dictated only by the total energy input with all other variables held constant. For the current thiol-ene samples, increasing the percent amplitude simultaneously increased the sample temperature (even in an ice bath), which led to larger particle
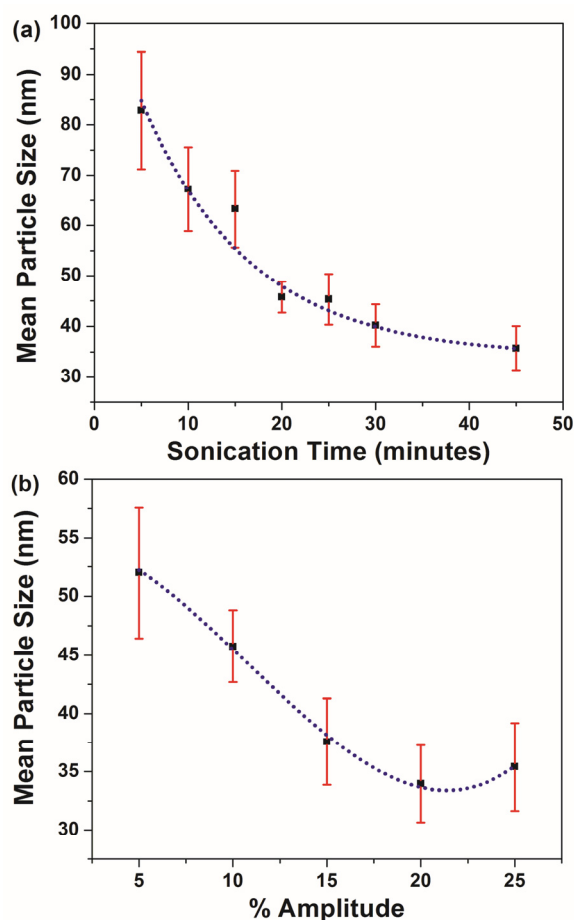


**Figure 8.** Effect of (a) sonication time (at 10% amplitude) and (b) percent amplitude (20 min ultrasonication time)  on particle size.  The blue dotted lines are not fits to the data and are inserted to guide the reader's eye. (Synthetic conditions: 20 mM SDS, 2.5 wt.% organic, 10 min UV exposure).
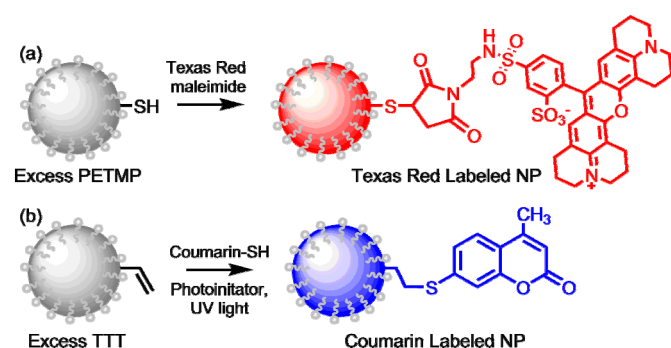
**Figure 9.** Postpolymerization modification of polythioether nanoparticles prepared with stoichiometric excess thiol or excess alkene *via* (a) thiol-Michael addition with Texas Red maleimide and (b) radical-mediated thiol-ene addition with 7-mercapto-4-methylcoumarin.

sizes for amplitudes greater than 20%. Thus, for the current sample volume and compositions, 10% amplitude and 20 minutes were chosen as the standard operating conditions to provide less variation between samples.

A salient feature that arises from the step-growth radical mechanism of thiol-ene photopolymerization is the ability to alter the reaction stoichiometry to achieve thiol-ene networks containing either excess thiol or alkene. The excess functional groups arising from non-stoichiometric photopolymerization conditions are then readily available for subsequent functionalization – an approach that was recently employed by Carlborg *et al.*[29] to fabricate thiol-ene microfluidic devices with functional surfaces. Likewise, Storha *et al.*[30] and Wang *et al.*[20] employed non-stoichiometric thiol-ene conditions to prepare particles with excess thiol and/or alkene on the surface, which were subsequently functionalized with fluorescent tags using various thiol-mediated modifications. Here, we exploit non-stoichiometric ratios of PETMP and TTT – neither of which readily undergo homopolymerization – to synthesize sub-100 nm thiol-ene nanoparticles with thiol or alkene functional surfaces in a simple, one-step process (Figure 9). Using similar formulations as previously described, the ratio of thiol to alkene was adjusted to either 2:1 for thiol functionalized nanoparticles, or 1:2 for alkene functionalized nanoparticles. These formulations were ultrasonicated to create the miniemulsion and cured with UV light, as previously described for stoichiometric samples (TEM of non-stoichiometric nanoparticles shown in Figure S4). Thiol and alkene functionalized nanoparticles were analyzed by solution ^{1}H NMR in $D_2O$ to confirm the presence of excess thiol and alkene available prior to functionalization (see Figure S5 and Figure S6). Likewise, the excess thiol and alkene functional groups were observed by FTIR (Figure S1). To demonstrate the simplicity of ligating pendent functional groups to the nanoparticle surface, nanoparticles presenting excess thiol on the surface were reacted with Texas Red C2 maleimide *via* thiol-Michael addition, while alkene functionalized nanoparticles were reacted with 7-mercapto-4-methylcoumarin *via* radical-mediated thiol-ene addition under UV light (10 min exposure). Nanoparticle dispersions were purified by multiple centrifugation wash steps following functionalization.
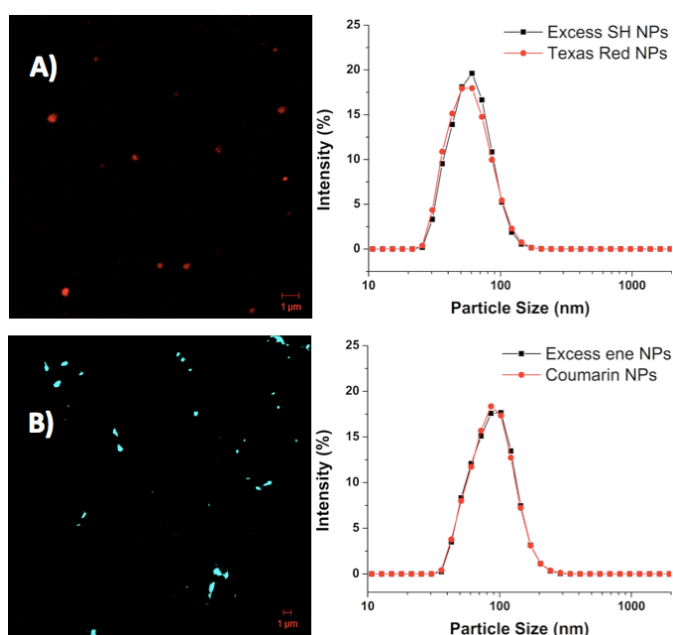


**Figure 10.** Fluorescence microscopy and particle size distributions of post-functionalized nanoparticles: a) 2:1 thiol:ene functionalized with Texas Red C2 maleimide b) 2:1 ene:thiol functionalized with 7-mercapto-4-methylcoumarin. DLS size distributions are shown before and after surface functionalization to illustrate the absence of particle agglomeration during the postmodification step. (Synthetic conditions: 20 mM SDS, 2.5 wt.% organic, 20 min ultrasonication at 10% amplitude, 10 min UV exposure).

Successful immobilization of both Texas Red and coumarin was confirmed by fluorescence microscopy, as shown in Figure 10. Importantly, DLS measurements collected before and after surface functionalization of the nanoparticles showed no change in particle size or evidence of nanoparticle agglomeration as a result of post-polymerization modification (Figure 10).

## Conclusion

In summary, crosslinked polythioether nanoparticles were prepared by radical-mediated thiol–ene miniemulsion photopolymerization. The effects of formulation (inhibitor, surfactant concentration, monomer weight fraction) and processing parameters (ultrasonication time and amplitude) on nanoparticle size were elucidated, enabling the facile synthesis of thiol-ene nanoparticles with mean particle sizes less than 100 nm. The step-growth nature of thiol-ene photopolymerization was exploited to prepare nanoparticles with thiol or alkene functional surfaces using non-stoichiometric monomer feeds. These thiol and alkene decorated nanoparticles provided a versatile platform for ligation of different functional moieties using thiol-Michael addition and thiol-ene addition, respectively, as simple, one-step postpolymerization modifications. We envision that thiol-ene miniemulsion polymerization can be exploited as a general method for the synthesis of functional polymer nanoparticles for a range of imaging, delivery, analysis, and coatings applications. Our current efforts are focused on extending this synthetic approach

to high solid content miniemulsions for more practical nanoparticle yields.

## Acknowledgements

## Notes and references

*a* School of Polymers and High Performance Materials

The University of Southern Mississippi

Hattiesburg, MS 39406

*b* Department of Biological Sciences

The University of Southern Mississippi

Hattiesburg, MS 39406

† Electronic Supplementary Information (ESI) available: Formulation tables, FTIR, light transmittance, additional TEM and confocal fluorescence images. See DOI: 10.1039/b000000x/

1. J. P. Rao and K. E. Geckeler, *Prog. Polym. Sci.*, 2011, **36**, 887-913.
2. J. M. Asua, *Prog. Polym. Sci.*, 2002, **27**, 1283-1346.
3. K. Landfester, *Angew. Chem. Int. Ed.*, 2009, **48**, 4488-4507.
4. C. Solans, P. Izquierdo, J. Nolla, N. Azemar and M. J. Garcia-Celma, *Curr. Opin. Colloid Interface Sci.*, 2005, **10**, 102-110.
5. M. Antonietti and K. Landfester, *Prog. Polym. Sci.*, 2002, **27**, 689-757.
6. D. Crespy and K. Landfester, *Beilstein J. Org.Chem.*, 2010, **6**, 1132-1148.
7. K. Landfester, F. Tiarks, H.-P. Hentze and M. Antonietti, *Macromol. Chem. Phys.*, 2000, **201**, 1-5.
8. F. Tiarks, K. Landfester and M. Antonietti, *J. Polym. Sci. Part A: Polym. Chem.*, 2001, **39**, 2520-2524.
9. J. M. Siebert, G. Baier, A. Musyanovych and K. Landfester, *Chem. Commun.*, 2012, **48**, 5470-5472.
10. R. Roux, L. Sallet, P. Alcouffe, S. Chambert, N. Sintes-Zydowicz, E. Fleury and J. Bernard, *ACS Macro Lett.*, 2012, **1**, 1074-1078.
11. C. E. Hoyle, T. Lee and T. Roper, *J. Polym. Sci. Part A: Polym. Chem.*, 2004, **42**, 5301-5338.
12. C. E. Hoyle and C. N. Bowman, *Angew. Chem. Int. Ed.*, 2010, **49**, 1540-1573.
13. C. E. Hoyle, A. B. Lowe and C. N. Bowman, *Chem. Soc. Rev.*, 2010, **39**, 1355-1387.
14. K. Y. van Berkel and C. J. Hawker, *J. Polym. Sci. Part A: Polym. Chem.*, 2010, **48**, 1594-1606.
15. J. Zou, C. C. Hew, E. Themistou, Y. Li, C.-K. Chen, P. Alexandridis and C. Cheng, *Adv. Mater.*, 2011, **23**, 4274-4277.
16. O. Z. Durham, S. Krishnan and D. A. Shipp, *ACS Macro Lett.*, 2012, **1**, 1134-1137.
17. O. Z. Durham and D. A. Shipp, *Polymer*, 2014, **55**, 1674-1680.
18. J. Tan, C. Li, J. Zhou, C. Yin, B. Zhang, J. Gu and Q. Zhang, *RSC Adv.*, 2014, **4**, 13334.
19. F. Jasinski, E. Lobry, B. Tarablsi, A. Chemtob, C. Croutxé-Barghorn, D. Le Nouen and A. Criqui, *ACS Macro Lett.*, 2014, **3**, 958-962.
20. C. Wang, M. Podgórski and C. N. Bowman, *Mater. Horiz.*, 2014.
21. J. C. Brown, P. N. Pusey and R. Dietz, *J. Chem. Phys.*, 1975, **62**, 1136-1144.
22. T. F. Tadros, M. Lemmens, B. Levecke and K. Booten, ed. T. F. Tadros, Wiley-VCH, 2008, vol. 4, pp. 35-50.
23. E. K. Skinner, F. M. Whiffin and G. J. Price, *Chem. Commun.*, 2012, **48**, 6800.
24. L. L. Hecht, C. Wagner, K. Landfester and H. P. Schuchmann, *Langmuir*, 2011, **27**, 2279-2285.
25. P. Jenkins and M. Snowden, *Adv. Colloid Interfac.*, 1996, **68**, 57-96.
26. N. Kiratzis, M. Faers and P. F. Luckham, *Colloids and Surfaces A: Physicochemical and Engineering Aspects*, 1999, **151**, 461-471.
27. K. Landfester, N. Bechthold, F. Tiarks and M. Antonietti, *Macromolecules*, 1999, **32**, 5222-5228.
28. T. Delmas, H. Piraux, A. Couffin, I. Texier, F. Vinet, P. Poulin, M. Cates and J. Bibette, *Langmuir*, 2011, **27**, 1683-1692.
29. C. F. Carlborg, T. Haraldsson, K. Oberg, M. Malkoch and W. van der Wijngaart, *Lab Chip*, 2011, **11**, 3136-3147.
30. A. Storha, E. A. Mun and V. V. Khutoryanskiy, *RSC Adv.*, 2013, **3**, 12275-12279.